Study of $In_xGa_{1-x}As/InAs_yP_{1-y}$ structures lattice mismatched to InP substrates

Dong-Su Kim and Stephen R. Forrest[a)]
Advanced Technology Center for Photonics and Optoelectronic Materials (ATC/POEM), Department of Electrical Engineering, Princeton University, Princeton, New Jersey 08544

Michael J. Lange, Marshall J. Cohen, and Gregory H. Olsen
Sensors Unlimited, 3490 U.S. Route 1, Princeton, New Jersey 08540

Ray J. Menna and Richard J. Paff
David Sarnoff Research Center, Princeton, New Jersey 08543

(Received 26 June 1996; accepted for publication 27 August 1996)

Material properties of several lattice-mismatched $In_xGa_{1-x}As/InAs_yP_{1-y}$ ($0.66<x<0.84$, $0.29<y<0.66$) alloys grown on InP substrates are investigated. The lattice constants and compositions were measured using x-ray diffraction and electron probe microanalysis. Photoluminescence, white light transmission, and detector cutoff wavelengths were used to determine the band gap of $In_xGa_{1-x}As$ as a function of In concentration x. The three methods agree to within 3%. The quality of the grown layers was also investigated using these techniques, in addition to cross-section transmission electron microscopy and Nomarsky optical microscopy. The dependence of the experimental measurements of band gap and lattice constant on material composition, measured by electron probe microanalysis, was compared against theoretical values. [S0021-8979(96)01823-3]

I. INTRODUCTION

Lasers and detectors that operate at wavelengths between 2 and 3 μm have numerous applications in gas sensing, lidar, windshear detection, spectroscopy, night vision, thermal imaging, etc.[1] Of the many different materials used for optoelectronic devices that operate at these wavelengths (e.g. HgCdTe, InSb, PtSi, etc.), $In_xGa_{1-x}As$ has demonstrated the highest performance and reliability.[1] InGaAs *p-i-n* detector arrays that operate at these wavelengths have widely been reported,[2–4] and recently an InGaAs avalanche photodiode with 2.1 μm cutoff wavelength has been demonstrated.[5] Lasers that operate at these wavelengths have also been reported.[6]

The biggest challenge for these devices is that in order to obtain $In_xGa_{1-x}As$ with a narrow band gap suitable for making devices that operate at wavelengths greater than 1.7 μm, the indium concentration x has to be greater than 0.53. This increases the lattice parameter of $In_xGa_{1-x}As$, thereby creating a lattice mismatch to the InP substrate. Growing mismatched material induces a high density of misfit dislocations at the material interface which act as recombination centers,[7] therefore degrading the performance of the optoelectronic devices. The most common means to deal with this problem is to grow $InAs_yP_{1-y}$ buffer layers between the InP substrate and the $In_xGa_{1-x}As$ ($x>0.53$) active layer.[3] In this scheme, the arsenic concentration in the buffer layer y is chosen such that the lattice parameter of $InAs_yP_{1-y}$ is identical to that of the adjacent $In_xGa_{1-x}As$ layer. In this way, the misfit dislocations are confined at the InP–$InAs_yP_{1-y}$ interface, and hence are located far from the active $In_xGa_{1-x}As$–$InAs_yP_{1-y}$ heterojunction, which ideally is lattice matched. The $InAs_yP_{1-y}$ buffer layers are often step graded, where the arsenic concentration is gradually increased in small increments (0.05–0.1) from InP to the appropriate composition of $InAs_yP_{1-y}$.[1] Buffer layers containing strained superlattices of $InAs_yP_{1-y}$ have also been employed.[4]

Even though these buffering schemes have been successful in decreasing the number of dislocations on the active $In_xGa_{1-x}As$ layers, to our knowledge there has not yet been a comprehensive study of the quality of the grown layers. Accurate information regarding the relationship between lattice constant and material composition of both $InAs_yP_{1-y}$ and $In_xGa_{1-x}As$ is needed to design and grow these mismatched structures with appropriate strain. Also, the band gap of $In_xGa_{1-x}As$ versus indium concentration must be established in order to make detectors and lasers with the desired wavelength response. Moon, Antypas, and James[8] proposed an empirical relationship for all compositions of $In_xGa_{1-x}As_yP_{1-y}$ based on parameters obtained from bulk materials. However, there has not been a comprehensive comparison of Moon and co-workers' formula against experimental data for lattice-mismatched materials grown on InP substrates. In this article we study the quality of the $In_xGa_{1-x}As$ layers using various experimental techniques, and also test the validity of Moon and co-workers formula against the experimental values of lattice constant and band gap obtained from different compositional structures of lattice-mismatched $InAs_yP_{1-y}$ and $In_xGa_{1-x}As$ grown on InP substrates. We confirm that most of the misfit dislocations are indeed contained within the $InAs_yP_{1-y}$ buffer layers, thus enabling the growth of $In_xGa_{1-x}As$ layers with a relatively small density of dislocations. Also, a more accurate relationship of lattice constant and band gap versus material composition is suggested.

a)Electronic mail: forrest@ee.princeton.edu

$InAs_{0.60}P_{0.40}$	1 μm	U/D
$In_{0.80}Ga_{0.20}As$	3 μm	U/D
$InAs_{0.60}P_{0.40}$	2 μm	U/D
$InAs_{0.55}P_{0.45}$	1 μm	U/D
$InAs_yP_{1-y}$ step graded layers		U/D
$InAs_{0.15}P_{0.85}$	1 μm	U/D
$InAs_{0.10}P_{0.90}$	1 μm	U/D
$InAs_{0.05}P_{0.95}$	1 μm	U/D, $n < 3 \times 10^{15} cm^{-3}$
InP Substrate		$n = 3 \times 10^{18} cm^{-3}$

FIG. 1. Schematic cross-section diagram of the material structure of a typical sample.

II. EPITAXIAL GROWTH AND MATERIALS CHARACTERIZATION

A schematic diagram of the material structure of a typical sample used in these studies is shown in Fig. 1. On a n^+ (3×10^{18} cm^{-3}) (100) InP substrate, a series of 1-μm-thick, step-graded, undoped buffer layers of $InAs_yP_{1-y}$ is grown with a 5% incremental increase of arsenic concentration between subsequent layers, with the stack progressing from InP to the final composition of $InAs_yP_{1-y}$. The value y of the final $InAs_yP_{1-y}$ buffer layer was varied from 0.3 to 0.6 among six different samples. Next, a 3-μm-thick, $In_xGa_{1-x}As$ active layer with lattice constant matched to the $InAs_yP_{1-y}$ directly underneath is grown. The structure was capped with a 1-μm-thick lattice-matched $InAs_yP_{1-y}$ layer. All grown layers were undoped, with a background free electron concentration of $n<3\times10^{15}$ cm^{-3}. The material was grown by chloride vapor phase epitaxy (VPE).[9] In this method, HCl gas carries the indium/gallium source metals into the hot zone of the horizontal gas reactor at 850–900 °C, thus forming metal chlorides. Then $AsCl_3$ and/or PCl_3 are combined in a mixing zone, followed by growth on the substrate maintained at ~700 °C. Growth rates can exceed 20 μm/h, and have been extensively used to produce detectors that operate in the wavelengths between 1 and 2 μm.[1]

The step grading buffer scheme has been chosen to minimize the number of dislocations in the $In_xGa_{1-x}As$ layer. The strain [defined as $\epsilon=(a_{ss}-a_{epi})/a_{ss}$, where a_{ss} and a_{epi} are lattice constants of the substrate and the grown layers, respectively] is chosen to be around 0.16% for each compositional grading step. It has been shown that in III–V materials, misfit dislocations begin to form for $\epsilon>10^{-4}$, but for lattice-mismatched steps with strain less than one percent, the dislocations are confined to within 3000 Å of the interface, thus enabling the growth of ''dislocation-free'' layers.[7] For strains much larger than 1%, dense arrays of threading dislocations which propagate along the growth direction can be observed.[9] Continuously graded samples also have dislocations that propagate continuously along the growth direction. This type of dislocation bends over at an abrupt compositional step,[7,9] suggesting that the step grading technique can minimize the number of defects in the $In_xGa_{1-x}As$ active layer.

Figure 2 shows an optical micrograph and profile of the surface of the grown wafer. The top surfaces of the materials were cross hatched, suggesting the existence of misfit dislocations. This cross hatching, however, does not necessarily mean that dislocations extend to the top layer, and has been observed even in samples where the misfit dislocations are confined to the first 3000 Å of a 125-μm-thick VPE-grown layer where no dislocations can be observed near the top of the epitaxial layer.[7] Dislocations at the first interface will affect the initial surface and this ''disturbance'' propagates as subsequent layers are grown, resulting in the rough surface morphology observed. The surface scan profile shows that the thickness variations are less than 3000 Å for a distance of 1000 μm across the surface of the wafer, and the root-mean-square roughness was calculated to be 800 Å. There was no significant difference in surface morphology between different samples.

Figure 3 shows cross-section transmission electron micrographs (TEM) of the $In_xGa_{1-x}As/InAs_yP_{1-y}$ interfaces. The $InP/InAs_yP_{1-y}$ heterojunction is shown in Fig. 3(a). A

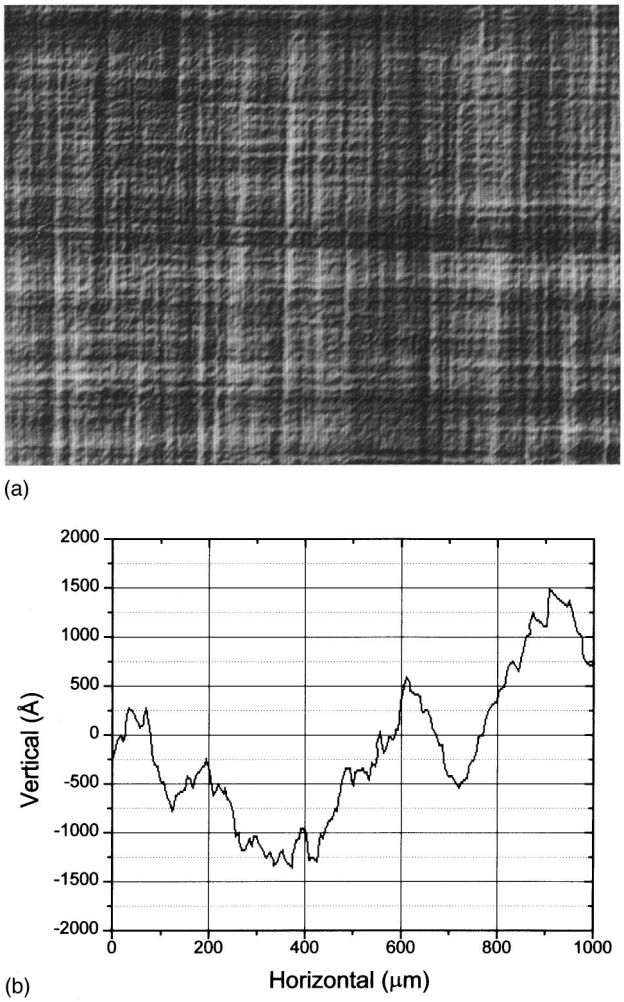

FIG. 2. Optical micrograph and surface profile of a typical sample.

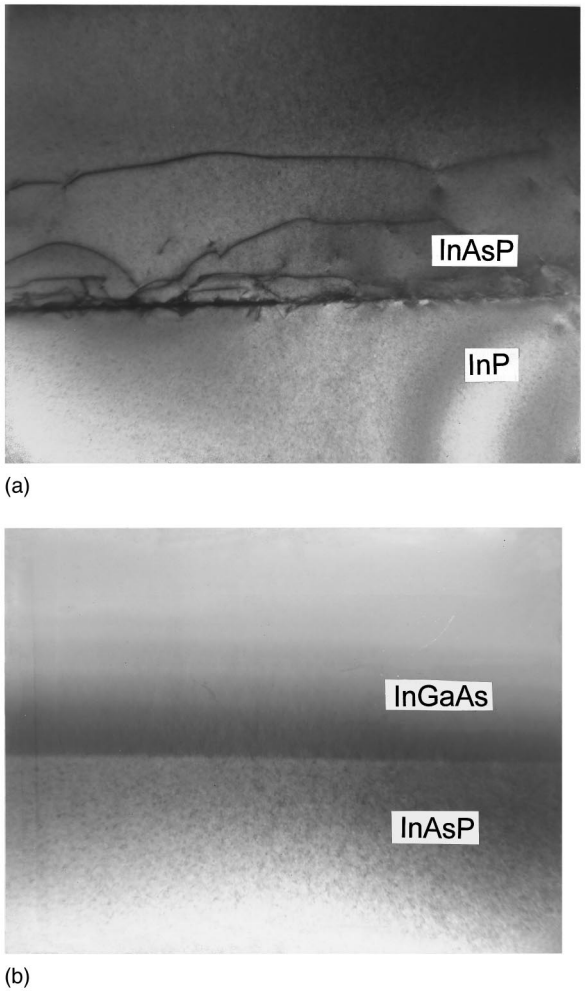

FIG. 3. Cross-sectional TEM micrograph of VPE-grown $In_xGa_{1-x}As/InAs_yP_{1-y}$ samples. (a) The $InP/InAs_yP_{1-y}$ heterojunction. A large number of dislocations can be observed, but they are confined to first 3000 Å of the $InAs_yP_{1-y}$ layer. (b) The $InAs_yP_{1-y}/In_xGa_{1-x}As$ junction. No dislocations can be observed.

large number of misfit dislocations can be observed at the $InP/InAs_yP_{1-y}$ interface layer, but most of the dislocations are confined to within 3000 Å of the junction. On the other hand, as shown in Fig. 3(b), no dislocations can be observed near the $InAs_yP_{1-y}/In_xGa_{1-x}As$ heterojunction. This demonstrates that the buffering scheme can indeed enable the growth of $In_xGa_{1-x}As$ layers lattice mismatched to the InP substrates with very few dislocations. This is consistent with earlier studies of other mismatched III–V materials.[9]

The compositions of the $InAs_yP_{1-y}$ and $In_xGa_{1-x}As$ layers were determined using electron-beam microanalysis directed along a bevel tapered at 1° from the wafer surface. A JEOL 733 electron microbeam prober was used for wavelength dispersive spectroscopy, and the data were analyzed using Tencor TASK software. The data were normalized so that the partial compositions (e.g., the concentration of As and P in $InAs_yP_{1-y}$) sum to one. The data were taken from two different regions of every wafer, and then averaged. For all wafers, the variation in composition from the different locations was less than 0.5%.

The lattice parameter was measured via x-ray diffraction with a Siemens B-5 x-ray diffractometer using the Cu $K\alpha$ line ($\lambda = 1.540\,598\,1$ Å). Figure 4 shows a scan of the (400) peaks of the $In_{0.83}Ga_{0.17}As/InAs_{0.66}P_{0.34}$ sample. The peaks were matched to the appropriate layers by comparing the (400) peaks to a (440) Berg–Barrett scan[10] which probes mostly the top $InAs_yP_{1-y}$ layer. Thus, in Fig. 4, the lattice constants of $In_{0.83}Ga_{0.17}As$ and $InAs_{0.66}P_{0.34}$ are measured to be $a_0 = 5.994$ and 6.000 Å, respectively. This suggests existence of strain between these two layers, but any effect of residual elastic strain in the layers is small, and hence is neglected. The sharpness of the peaks demonstrates good crystallinity of these layers, but quantitative analysis of the peak width is limited due to the resolution of the single crystal x-ray source used.

Three different methods were used to determine the band gap of the $In_xGa_{1-x}As$ layer. First, the wavelength-dependent photoluminescence (PL) was done using a $\lambda = 514$ nm Ar ion laser. The penetration depth of the laser beam into the $InAs_yP_{1-y}$ layer is on the order of 2000 Å, but high internal radiative recombination efficiencies (25%–50%) were measured from the $In_xGa_{1-x}As$ layers due to the long diffusion length (~ 1 μm) of the $InAs_yP_{1-y}$ layers. The de-

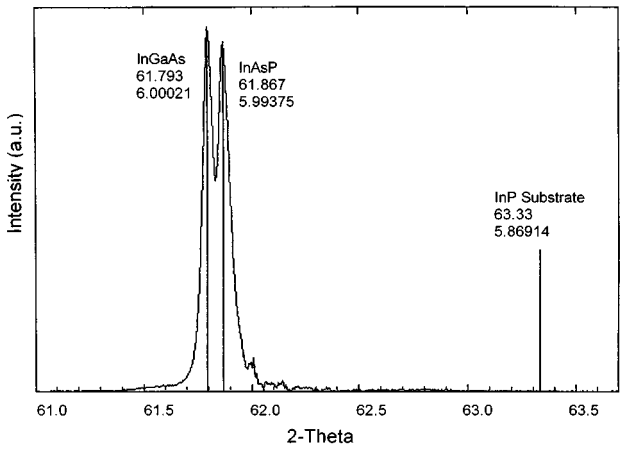

FIG. 4. X-ray scan for an $In_{0.83}Ga_{0.17}As/InAs_{0.66}P_{0.34}$ sample for (400) peaks.

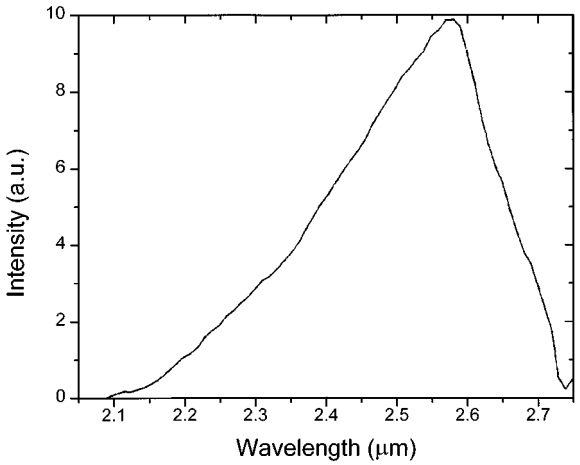

FIG. 5. Wavelength-dependent photoluminescence spectrum of an $In_{0.83}Ga_{0.17}As/InAs_{0.66}P_{0.34}$ sample with 2.6 μm peak.

tails of the PL setup and the efficiency experiments are described elsewhere.[11] A PL spectrum for a sample with a luminescence peak at 2.6 μm is shown in Fig. 5. In order to obtain the band gap from the spectra, a correction for the carrier energy distribution must be made. That is, the maximum of PL is at energy $E_{\mathrm{PL}}=E_g+E_{kT}$, where E_g is the actual bandgap and $E_{kT}=kT/2$ (k is Boltzmann's constant and T is the temperature) is the energy at which the product of the conduction-band density of states $[N(E)\sim E^{1/2}]$ and the Boltzmann distribution function $[\exp(-E/kT)]$ as the function of energy E reaches its maximum. The shape of the PL spectrum should have the shape of the product of these two functions. This relationship gives a full width half-maximum (FWHM) of 45 meV at room temperature. From Fig. 5 the FMHM is measured to be 49 meV. This sharpness of the PL spectra again demonstrates the good crystal quality and homogeneity of the $In_xGa_{1-x}As$ layer. The integrated PL intensity was also measured and the internal efficiencies of the samples were calculated to be greater than 25% and up to 50%.[11] Such high radiative recombination efficiencies at room temperature for narrow-band-gap materials are unexpected, and demonstrate excellent quality of the $In_xGa_{1-x}As$ layers.

In a second measurement of the band gap, the wavelength-dependent transmission coefficient was measured by illuminating the sample with a white light source through a spectrometer and then measuring the intensity of

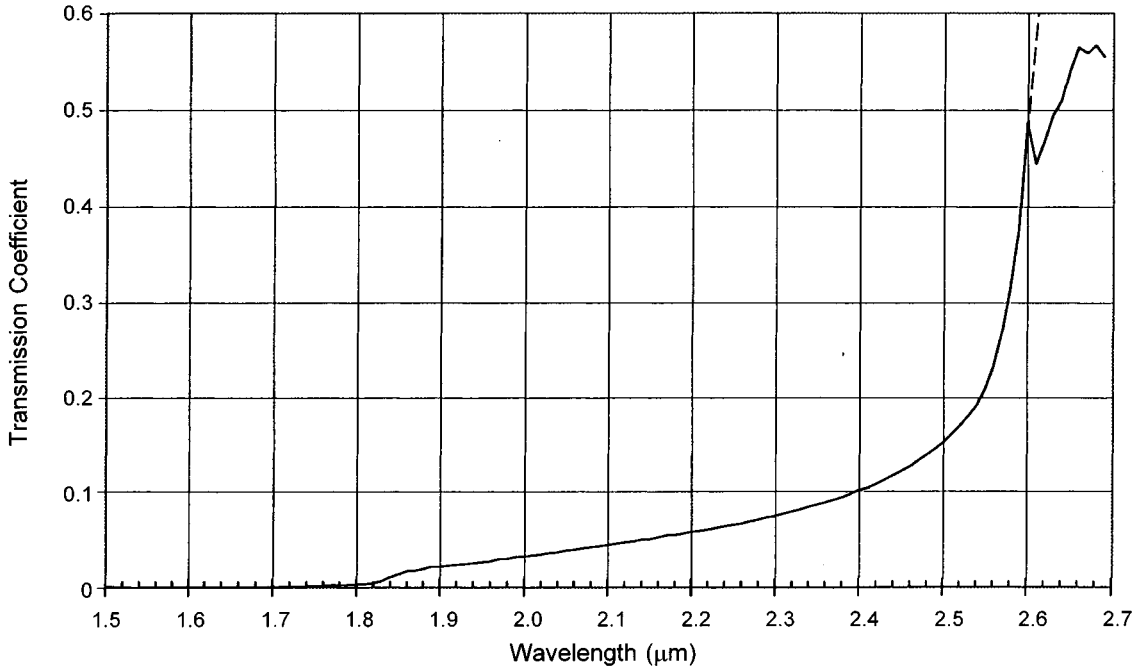

FIG. 6. Transmission coefficient vs wavelength for an $In_{0.83}Ga_{0.17}As/InAs_{0.66}P_{0.34}$ sample with 2.62 μm band gap.

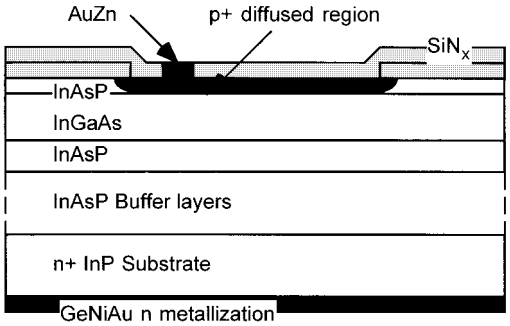

FIG. 7. Diagram of the *p-i-n* photodiode fabricated from the epitaxial material.

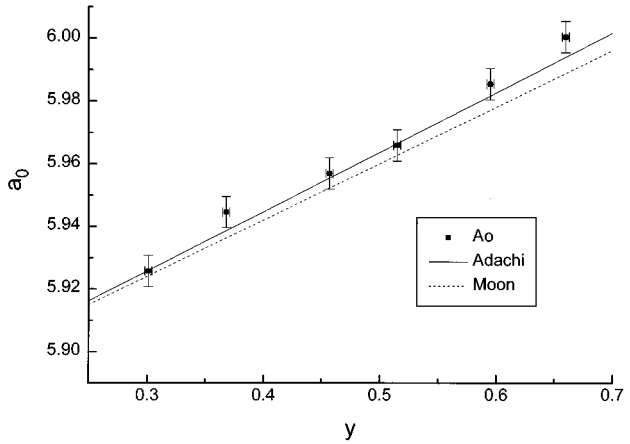

FIG. 8. Lattice constant vs composition for $InAs_yP_{1-y}$ layers. The points are from x-ray data, and the lines are from theoretical values predicted by formula from Refs. 8 and 13.

the transmitted light using a calibrated detector. This curve was divided by the spectral dependent intensity of the light source to obtain the transmission coefficient. Figure 6 shows the transmission coefficient versus wavelength for a sample with 2.62 ± 0.02 μm band-gap cutoff wavelength. The band gap was determined by linearly extrapolating the curve from the inflection point to the maximum value of the transmission coefficient, as shown by the dotted lines in Fig. 6.

Finally, *p-i-n* photodiodes were fabricated with these samples by diffusing zinc through the top $InAs_yP_{1-y}$ layer using a SiN_x mask. The substrate was lapped and Ge/Ni/Au *n*-type and Au/Zn *p*-type metal contacts were deposited using e-beam evaporation. The device was then sealed in a hermetic package. The fabrication process is similar to that used for conventional detectors, and the details can be found in Ref. 1. Figure 7 shows the schematic diagram of the detector. The wavelength response of the detector was measured in a setup similar to that used in the transmission experiments, except that the photocurrent from the $In_xGa_{1-x}As/InAs_yP_{1-y}$ detector was compared against that of the output of a calibrated detector. The band gap was determined by the cutoff wavelength using the same method as employed for the transmission coefficient experiment.

The above measurements were done at room temperature, and Table I lists the experimental results for all of the samples studied.

III. LATTICE CONSTANT AND BAND GAP VERSUS MATERIAL COMPOSITION

In Fig. 8 the experimental values of lattice constant of $InAs_yP_{1-y}$ versus the arsenic concentration y are plotted and compared with the theoretical calculations. The lattice constant of ternary III–V alloys varies linearly with material composition (Vegard's law[12]). Moon and co-workers[8] used $a_0=5.87$ and 6.05 Å as lattice parameters of InP and InAs, respectively to derive $a_0(\text{Å})=5.87+0.18y$. Using more accurate values for the lattice parameters of InP and InAs of $a_0=5.8688$ and 6.0584 Å, compiled by Adachi,[13] one can derive $a_0(\text{Å})=5.8688+0.1896y$. Both equations are plotted in Fig. 8, but the formula using Adachi's values provides a better fit to the data ($\chi^2=0.750$ vs 2.446 for Moon and co-workers' formula[8]).

The lattice constant of the $In_xGa_{1-x}As$ active layer versus material composition is plotted in Fig. 9. As in the case for $InAs_yP_{1-y}$, the expression using more accurate end-point values [$a_0(\text{Å})=5.6533+0.4051x$; $\chi^2=2.048$] provides a better fit to the data than does Moon and co-workers' formula[8] [$a_0(\text{Å})=5.65+0.40x$; $\chi^2=2.813$]. The effect from any residual elastic strain in the material is very small ($<0.3\%$), and thus is neglected. The above results confirm the validity of Vegard's law for these lattice-mismatched $InAs_yP_{1-y}/In_xGa_{1-x}As$ samples.

The measured values of band gap of $In_xGa_{1-x}As$ from three different experimental techniques are plotted in Fig. 10. For convenience, the y axis is plotted in both μm and eV. It is generally assumed that the band gap versus concentration follows a quadratic relationship (see, e.g., Ref. 8) such as $E_g=ax+b(1-x)+cx(1-x)$. Here, a and b are band-gap

TABLE I. Experimental data for lattice-mismatched $InAs_yP_{1-y}/In_xGa_{1-x}As$ samples grown on InP substrate.

Sample	1	2	3	4	5	6
y, electron μprobe	0.457	0.301	0.595	0.368	0.515	0.660
a_0 (InAsP), XRD[a] (Å)	5.957	5.926	5.985	5.945	5.966	6.000
x, electron μprobe	0.731	0.663	0.789	0.706	0.745	0.833
a_0 (InGaAs), XRD (Å)	5.941	5.913	5.978	5.942	5.946	5.994
E_{pl}, PL (μm)	2.18	1.99	2.41	2.11	2.26	2.57
$E_{\text{pl}}-E_{kT}$ (μm)	2.23	2.03	2.47	2.16	2.31	2.64
E_g, transmission (μm)	2.20	2.00	2.46	2.14	2.32	2.62
E_g, detector cutoff (μm)	2.19	1.98	2.44	2.11	2.29	2.59

[a]Designates X-ray diffraction.

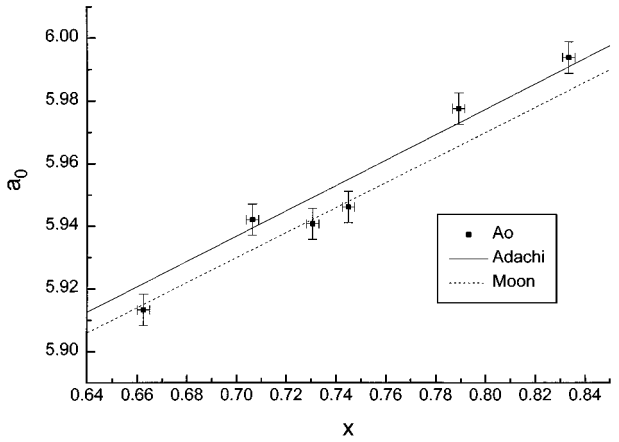

FIG. 9. Lattice constant vs material composition for $In_xGa_{1-x}As$ layers. The points are from x-ray data, and the lines are from theoretical values predicted by formula from Refs. 8 and 13.

energies of the binary end points (E_g of InAs and GaAs, respectively, for $In_xGa_{1-x}As$), and c, which is called the ''bowing parameter,'' is determined by the amount of deviation from linearity. Moon and co-workers used 0.35 and 1.42 eV as the band gaps of InAs and GaAs, respectively, and 0.478 was used as the bowing parameter. The line obtained using these values is also plotted in Fig. 10. The more recent data compiled by Adachi[13] suggest that the room-temperature band gap of InAs is closer to 0.36 eV. If we use that value to fit the quadratic function to the PL data, we obtain $c=0.479\pm0.010$, with $\chi^2=0.414$. The resulting line from the fit,

$$E_g=0.36x+1.42(1-x)-0.479x(1-x),$$

is also plotted in Fig. 10. This relationship compares well with other published results for unstrained $In_xGa_{1-x}As$.[14]

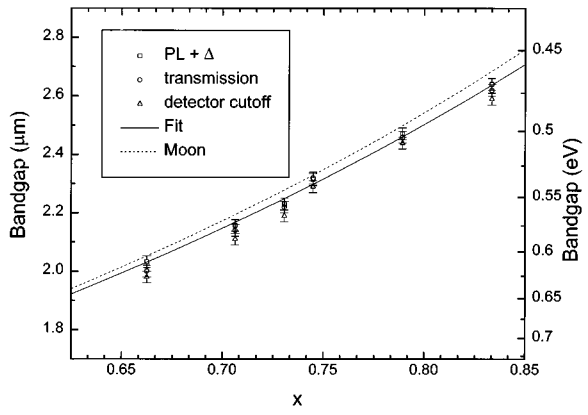

FIG. 10. Band gap vs material composition for $In_xGa_{1-x}As$. Data points are from PL, transmission, and detector cutoff measurements, and the lines are from Moon and co-workers (Ref. 8) (dotted line) and fit using values from Adachi (Ref. 13).

TABLE II. Fitting constants for the band gaps and lattice constants obtained for $InAs_yP_{1-y}$ and $In_xGa_{1-x}As$.

	Lattice constant (Å)	Band gap (eV)
InP	5.8688	
InAs	6.9584	0.36
GaAs	5.6533	1.42

Fitting constants for the bandgaps and lattice constants obtained for $InAs_yP_{1-y}$ and $In_xGa_{1-x}As$ are compiled for reference in Table II.

IV. CONCLUSION

A materials study of several $In_xGa_{1-x}As/InAs_yP_{1-y}$ ($0.66<x<0.84$, $0.29<y<0.66$) lattice-mismatched layers grown on InP substrates was performed. Investigations using cross-section TEM, Nomarsky optical microscopy, x ray, and PL reveal good quality $In_xGa_{1-x}As/InAs_yP_{1-y}$ layers with few misfit dislocations. The relationship of the lattice constant measured using x-ray diffraction versus material composition measured by electron probe microanalysis confirms the validity of Vegard's law for these mismatched materials. In addition to PL, white light transmission and detector cutoff wavelength measurements were used to determine the band gap of the samples, and updated relationships using more recent materials parameters of InAs are suggested by our curve fits. These results should be very useful in the design and growth of lattice-mismatched $In_xGa_{1-x}As$ ($x>0.53$) detectors and lasers with high quantum efficiencies and low leakage currents.

ACKNOWLEDGMENTS

The authors acknowledge a grant from the Office of Naval Research and NASA/JPL Small Business Innovative Research (SBIR) contract for support of this work. Sumitomo Electric, Inc. graciously provided the VPE-grown epitaxial layers.

[1] G. H. Olsen, Laser Focus World **27**, A21 (1991).
[2] G. H. Olsen, A. M. Joshi, S. M. Mason, K. M. Woodruff, E. Mykietyn, V. S. Ban, M. J. Lange, J. Hladky, G. C. Erickson, and G. A. Gasparian, Proc. SPIE **1157**, 276 (1989).
[3] D.-S. Kim, S. R. Forrest, M. J. Lange, G. H. Olsen, and M. J. Cohen, IEEE Photonics Technol. Lett. **PTL-6**, 235 (1994).
[4] M. Wada and H. Hosomatsu, Appl. Phys. Lett. **64**, 1265 (1994).
[5] D.-S. Kim, S. R. Forrest, G. H. Olsen, M. J. Lange, R. U. Martinelly, and N. J. Di Giuseppe, in *IEEE/LEOS Conference on Lasers and Electro-Optics*, 1995, CPD32.
[6] R. U. Martinelli, T. J. Zamerowski, and P. A. Longeway, Appl. Phys. Lett. **54**, 277 (1989).
[7] G. H. Olsen, J. Cryst. Growth **31**, 223 (1975).
[8] R. L. Moon, G. A. Antypas, and L. W. James, J. Electron. Mater. **3**, 635 (1974).
[9] G. H. Olsen and T. J. Zamerowski, Prog. Cryst. Growth Charact. **2**, 309 (1979).
[10] J. Newkirk, Trans. AIME **215**, 483 (1959).
[11] D. Garbuzov, D.-S. Kim, S. R. Forrest, R. Menna, M. Lange, G. H. Olsen, and M. Cohen, J. Electron. Mater. (to be published).
[12] E. F. Hockings, I. Kudman, T. E. Seidel, C. M. Schmelz, and E. F. Steigmeier, J. Appl. Phys. **37**, 2879 (1966).
[13] S. Adachi, J. Appl. Phys. **53**, 8775 (1982).
[14] R. E. Nahory, M. A. Pollack, and W. D. Johnston, Jr., Appl. Phys. Lett. **33**, 659 (1978).